Nano Energy 34 (2017) 1–7

Contents lists available at ScienceDirect

Nano Energy

journal homepage: www.elsevier.com/locate/nanoen

Communication

In situ segregation of cobalt nanoparticles on VN nanosheets *via* nitriding of $Co_2V_2O_7$ nanosheets as efficient oxygen evolution reaction electrocatalysts

Xiang Peng[a], Lei Wang[b], Liangsheng Hu[c], Yong Li[c], Biao Gao[d], Hao Song[d], Chao Huang[a,d], Xuming Zhang[d], Jijiang Fu[d], Kaifu Huo[b,*], Paul K. Chu[a,*]

[a] Department of Physics and Materials Science, City University of Hong Kong, Tat Chee Avenue, Kowloon, Hong Kong, China
[b] Wuhan National Laboratory for Optoelectronics, Huazhong University of Science and Technology, Wuhan 430074, China
[c] Department of Applied Biology and Chemical Technology and the State Key Laboratory of Chirosciences, The Hong Kong Polytechnic University, Hung Hom, Kowloon, Hong Kong, China
[d] The State Key Laboratory of Refractories and Metallurgy, Wuhan University of Science and Technology, Wuhan 430081, China

ARTICLE INFO

Keywords:
Cobalt nanoparticles
VN nanosheets
In situ segregation
Water splitting
Oxygen evolution reaction

ABSTRACT

Metallic Cobalt nanoparticles segregated *in situ* on conductive vanadium nitride (Co/VN) nanosheets synthesized by ammonia nitridation of hydrothermally prepared $Co_2V_2O_7$ nanosheets are investigated as high-performance oxygen evolution reaction (OER) electrocatalysts. The metallic Co nanoparticles with a large number of exposed active sites are distributed uniformly and adhere firmly to the VN substrate to enhance the OER efficiency, facilitate fast charge transfer, and improve the stability. As a result, a small overpotential of 320 mV is required to achieve a current density of 10 mA cm^{-2} with a small Tafel slope of 55 mV dec^{-1}. The excellent stability is indicated by an overpotential shift of only 34 mV after 2000 cyclic voltammetry cycles at a large current density of 200 mA cm^{-2}. The precious-metal-free Co/VN nanosheets deliver outstanding OER performance and are promising as electrocatalysts in water splitting and related applications.

1. Introduction

The oxygen evolution reaction (OER) is a half-cell reaction coupled with the hydrogen evolution reaction in water splitting provides a clean and sustainable energy source instead of fossil fuels [1–3]. However, the inefficiency of available electrocatalysts for OER is one of the obstacles hampering wide application of water splitting in the industry because the critical step in four-electron oxidation *via* the reaction of $4OH^- \rightarrow 2H_2O+4e^-+O_2$ often requires a high overpotential (η) in order to attain the desired current density. Although some noble metals such as nanostructured Ir and Ru and their oxides have been reported to have relatively low overpotentials in OER in aqueous acidic and basic solutions, the rare abundance and high price do not bode well for large-scale industrial production [4–9]. Recently, a common transition metal, cobalt, and its oxide/hydroxide have shown good OER performance [10–16]. However, the insufficient electronic conductivity of Co-based oxide/hydroxide hinders further development and improvement as OER electrocatalysts.

A strategy to improve the OER activity of Co-based electrocatalysts is to combine the electrocatalysts with other highly conductive materials such as carbon-based nanomaterials [10,17,18] and metals [19,20], and it has been shown that the OER performance of Co-based electrocatalysts can be improved effectively when combining with a conductive substrate. However, the Co-based electrocatalysts are typically distributed randomly on the conductive agent without tight adhesion and coupling thereby resulting in high contact resistance and compromised OER activity. In some serious cases, loss or aggregation of the catalysts can shorten the lifetime. Therefore, it is important to design and produce a novel structure composed of the highly active Co-based electrocatalyst on a conductive substrate with firm adhesion/bonding in order to reduce the contact resistance as well as loss and aggregation so as to enhance the OER performance.

Vanadium nitride (VN) has been used as the support for precious metal electrocatalysts such as Pt and Pd [21,22] due to the metallic properties, resistance to most chemical solvents, and stability under a wide variety of conditions [23,24]. According to previous reports, formation of the V-N bond at 500–550 °C is easier than the Co–N bond at 850 °C, below which metallic Co is formed by ammonia nitridation of the corresponding oxides [25–28]. Hence it is feasible to segregate metallic Co *in situ* from cobalt vanadate composed of Co–

* Corresponding author.
E-mail addresses: kfhuo@hust.edu.cn (K. Huo), paul.chu@cityu.edu.hk (P.K. Chu).

http://dx.doi.org/10.1016/j.nanoen.2017.02.016
Received 23 January 2017; Received in revised form 8 February 2017; Accepted 11 February 2017
Available online 12 February 2017

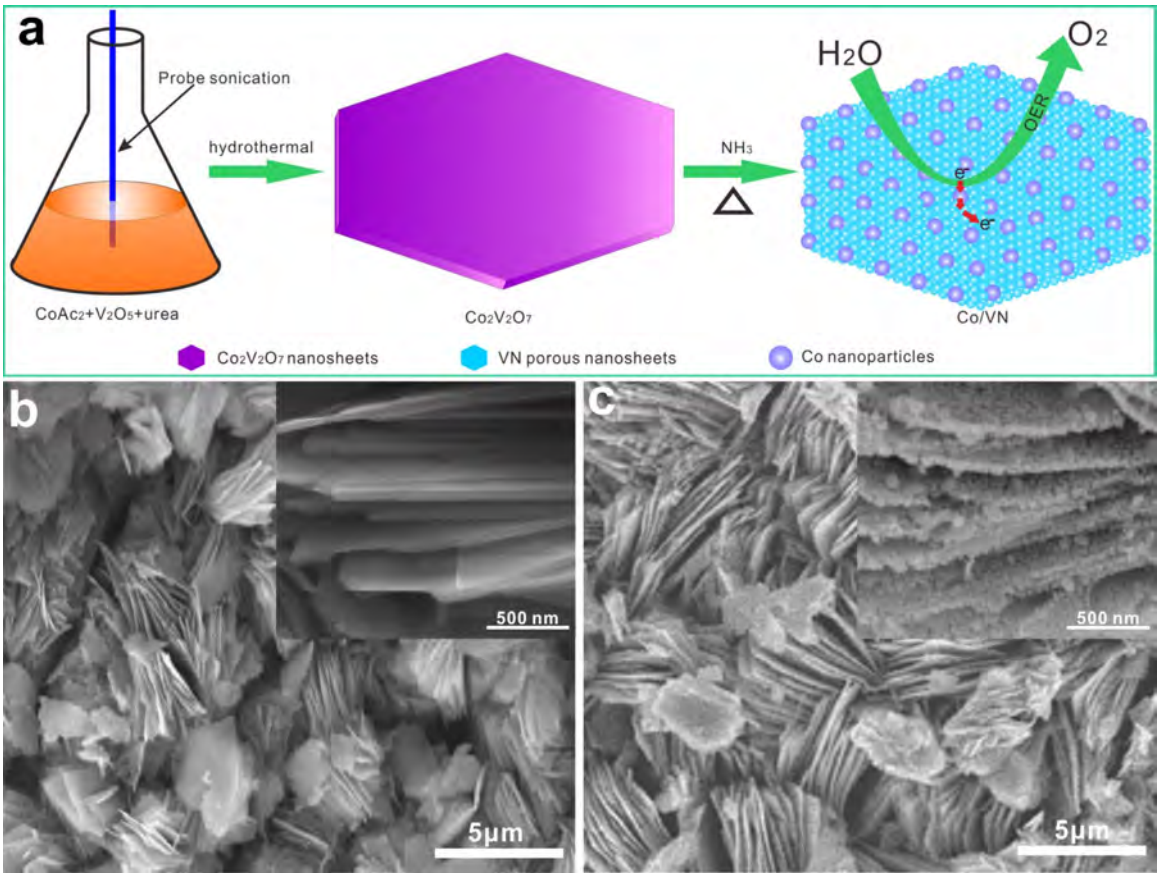

Fig. 1. (a) Schematic illustration of the preparation procedures of the porous Co/VN nanosheets electrocatalyst for high-performance OER; SEM images of (b) hydrothermal product $Co_2V_2O_7$ and (c) Co/VN with insets showing the corresponding high-magnification images.

O and V–O bonds after ammonia nitridation in order to form the metallic Co embedded VN composite at the suitable temperature. Co atoms segregated from cobalt vanadate should bond with the VN substrate firmly and be distributed on the VN uniformly at certain locations to ensure small contact resistance while preventing Co from falling off and aggregating. Generally, metallic Co on the surface is oxidized to oxide/hydroxide [Co(IV)] with OER activity similar to that of metallic Co [29] as a core-shell structure comprising conductive metallic Co constitutes the core facilitating fast charge transfer and further improving the OER activity.

In this work, metallic Co nanoparticles are segregated and synthesized *in situ* on VN (Co/VN) nanosheets by a hydrothermal method followed by ammonia nitridation as schematically illustrated in Fig. 1a. The metallic Co nanoparticles are distributed uniformly and have strong adhesion with the VN substrate. The novel structure shows ultra-fast electron transfer and excellent OER activity including a small overpotential, long lifetime, and small Tafel slope suggesting large potential in water splitting and related applications.

2. Experimental section

2.1. Samples preparation

The $Co_2V_2O_7$ nanosheets were synthesized by a hydrothermal method. 120 mg of the V_2O_5 powders (Sigma-Aldrich), 500 mg of $Co(Ac)_2{\cdot}4H_2O$ (Sigma-Aldrich), and 120 mg of urea (Sigma-Aldrich) were added to 40 mL of deionized water (DW) under sonication (SCIENTZ-IID Ultrasonic Homogenizer, Ningbo Scientz Biotechnology Co., Ltd., China) for 20 min. It was followed by a hydrothermal reaction at 120 °C for 3 h in a 50 mL Teflon-lined autoclave. After cooling, the product was washed several times and vacuum dried overnight. The metallic Co nanoparticles embedded VN nanosheets (Co/VN) were prepared by nitriding the as-prepared $Co_2V_2O_7$ in NH_3 at 550 °C for 3 h in a tube furnace. For comparison, pure metallic Co was prepared by similar hydrothermal and nitridation processes but without V_2O_5 as the precursor. The pure VN nanosheets was prepared according to the procedures described in our previous paper [30]. The mixture of metallic Co and VN nanosheets (Co+VN) was prepared by mixing metallic Co and VN directly with a molar ratio of 1:1.

2.2. Materials characterization

The morphology and microstructure of the samples were determined by scanning electron microscopy (SEM, FEI Nova 400 Nano), X-ray diffraction (XRD, Bruker AXS D2 Phaser) with Cu K_α radiation in the range of 10–90° (2θ), transmission electron microscopy (TEM) and high-resolution TEM (HR-TEM) equipped with energy-dispersive X-ray spectroscopy (TEM, FEI Titan G2), and X-ray photoelectron spectroscopy (XPS, ESCALB MK-II, VG Instruments, UK) using monochromatic Mg K_α X-ray. The specific surface area and porous structure were evaluated by the Brunauer-Emmett-Teller (BET) and Barrett-Joyner-Halenda (BJH) methods on the Micromeritics ASAP 2020 at 77 K.

2.3. Electrochemical measurements

The commercial IrO_2 catalyst was purchased from Sigma-Aldrich. The electrochemical measurements were carried out on a three-electrode system (CHI 6144D, Shanghai CH Instruments Company, China) with a Pt foil as the counter electrode, saturated calomel electrode (SCE) as the reference electrode, and modified glassy carbon

electrode (GCE) as the working electrode. The SCE was calibrated referenced to the reversible hydrogen electrode (RHE) in a hydrogen saturated electrolyte with a Pt wire as the working electrode as shown in Fig. S1. All the potentials were referenced to RHE according to the equation: $E_{RHE}=E_{SCE}+1.018$ V. The working electrode was prepared as follows. Twelve mg of the as-prepared sample were dispersed in 3 mL of DW under sonication and 5 μL of the dispersion were loaded on a GCE with a diameter of 3 mm at a loading of 0.28 mg cm^{-2}. After drying in air, 5 μL of the 0.5% nafion-water-ethonal solution covered the GCE to fix the electrocatalyst. The OER activity was evaluated by linear sweep voltammetry (LSV) at a scanning rate of 5 mV s^{-1}. The electrochemical impedance spectra (EIS) were acquired at 0.6 V *vs.* SCE with an ac perturbation of 5 mV in the frequency range between 100 kHz and 0.1 Hz. The stability of the electrocatalyst was evaluated by cyclic voltammetry (CV) at a scanning rate of 200 mV s^{-1}. All the potentials in the polarization curves and Tafel plots were *iR* corrected using R_s obtained in EIS. The measurements were conducted at room temperature in 1 M KOH solution.

3. Results and discussion

Fig. 1a presents the schematic illustration of the synthesis of the porous Co/VN nanosheets electrocatalyst. The $Co_2V_2O_7$ nanosheets are produced by a low-temperature (120 °C) hydrothermal method using $Co(Ac)_2{\cdot}4H_2O$, V_2O_5, and urea as precursors. During subsequent ammonia nitridation, the $Co_2V_2O_7$ nanosheets are converted into porous VN nanosheets embedded with metallic Co nanoparticles uniformly due to *in situ* segregation of Co from $Co_2V_2O_7$. The high dispersity and tight bonding with the VN substrate prevent the metallic Co nanoparticles from falling off and aggregating thus producing a large number of stable and exposed active sites. They also provide fast transportation paths for electrons due to the small contact resistance.

Fig. 1b shows the SEM images of the hydrothermal product of $Co_2V_2O_7$ with the nanosheets structure and a smooth surface. After ammonia nitridation at 550 °C for 3 h (Figs. 1c and S2), the nanosheet morphology is retained but the surface becomes rough with many nanoparticles embedded in the porous nanosheets, indicating that some nanoparticles are segregated on the nanosheets surface and the nanosheets become porous after ammonia nitridation. To determine the phases and composition of the ammonia nitridation products, XRD is performed as shown in Fig. 2a. The hydrothermal product can be indexed to $Co_2V_2O_7$ (JCPDS 70-1189) and the crystallinity is improved after annealing in air to remove water as shown in Fig. S3. Ammonia nitridation of the hydrothermal product was performed at different temperature and for different time and the XRD patterns are shown in Fig. S4. When the annealing temperature is less than 550 °C and time is below 3 h, some vanadate species still remain. When the annealing temperature is higher than 550 °C and time is more than 3 h, all the diffraction patterns (Figs. S4 and 2a) match those of VN (JCPDS 73-0528) and metallic Co (JCPDS 15-0806) [31] revealing that a composite composed of VN and metallic Co is produced. For comparison, the pristine V_2O_5 powders are subjected to the same ammonia nitridation process and the diffraction patterns (Fig. 2a) can be indexed to VN (JCPDS 73-0528) in agreement with previous results [27,30]. Fig. S5 shows the XRD pattern of the product prepared by a similar hydrothermal process and ammonia nitridation but without V_2O_5 as the precursor confirming that pure metallic Co (JCPDS 15-0806) has been produced.

XPS is conducted to determine the composition of the ammonia nitrided product and the data are exhibited in Fig. 2b and c. The high-resolution V 2p3/2 peak (Fig. 2b) can be fitted with three peaks at 514.1, 515.4, and 517.0 eV corresponding to V-N, VNO, and V-O, respectively. The oxygen-containing species stemming from slight surface oxidation of VN [32–35]. The Co 2p3/2 XPS (Fig. 2c) can be attributed to metallic Co, cobalt oxides [Co(II) and Co(III)], and satellite signals [36–38]. The cobalt oxide species, which are not detected by XRD as only metallic Co is observed, shows strong signal in XPS. To identify the state and distribution of cobalt in the composite in more details, TEM and HR-TEM are conducted as shown in Fig. 3a–d. The TEM images in Fig. 3a and b confirm that the nitrided product, Co/VN, has a porous nanosheet structure embedded with many nanoparticles ranging from 50 to 80 nm in size. The HR-TEM image in Fig. 3c illustrates porous nanosheets with a neighboring lattice fringes spacing of 0.242 nm corresponding to the (111) crystal planes of VN (JCPDS 73-0528). The embedded nanoparticles have a core-shell structure with the core showing neighboring lattice fringes of 0.201 nm and 0.176 nm associated with the (111) and (200) crystal planes of metallic Co (JCPDS 15-0806) respectively, as shown in Fig. 3d. Around the metallic Co core, there is an amorphous shell with several nanometers in thickness. To identify the amorphous layer, elemental mapping is carried out as shown in Fig. 3e which shows a strong O signal around metallic Co due to the oxide layer due to surface oxidation. The results suggest metallic Co nanoparticles with an oxide layer are embedded in the porous VN nanosheets by ammonia nitridation of the hydrothermal product $Co_2V_2O_7$. The specific surface area and pore-size distribution of the Co/VN porous nanosheets are determined and shown in Fig. S6. The BET specific surface area is 37 m^2 g^{-1} and BJH pore-size is ~2.5 nm (Fig. S6b), compared to a value of 21 m^2 g^{-1} for the sample before ammonia nitridation ($Co_2V_2O_7$). The peak at 30–100 nm in Fig. S6b matches the size of the embedded metallic Co nanoparticles observed by TEM.

The electrocatalytic performance of the porous Co/VN nanosheets in OER is evaluated by LSV in 1 M KOH using a three-electrode configuration. All the potentials in the polarization curves and Tafel plots are *iR* corrected as illustrated in Fig. S7. The polarization curves of Co/VN and $Co_2V_2O_7$ in comparison with commercial IrO_2 and bare GCE are presented in Fig. 4a. The overpotential at a current density of 10 mA cm^{-2}, which is a metric relevant to solar fuel synthesis and commonly used to evaluate the OER activity [39], is 320 mV for Co/VN (Table 1) and smaller than those of the hydrothermal product $Co_2V_2O_7$

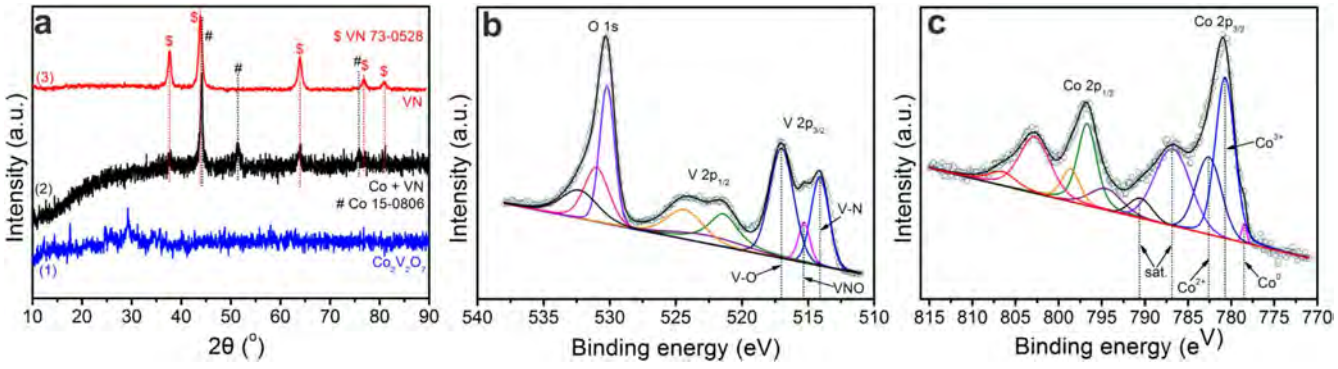

Fig. 2. (a) XRD patterns of (1) hydrothermal product $Co_2V_2O_7$, (2) Co/VN, and (3) VN. High-resolution XPS of V2p-O1s (b) and Co2p (c) for Co/VN electrocatalyst.

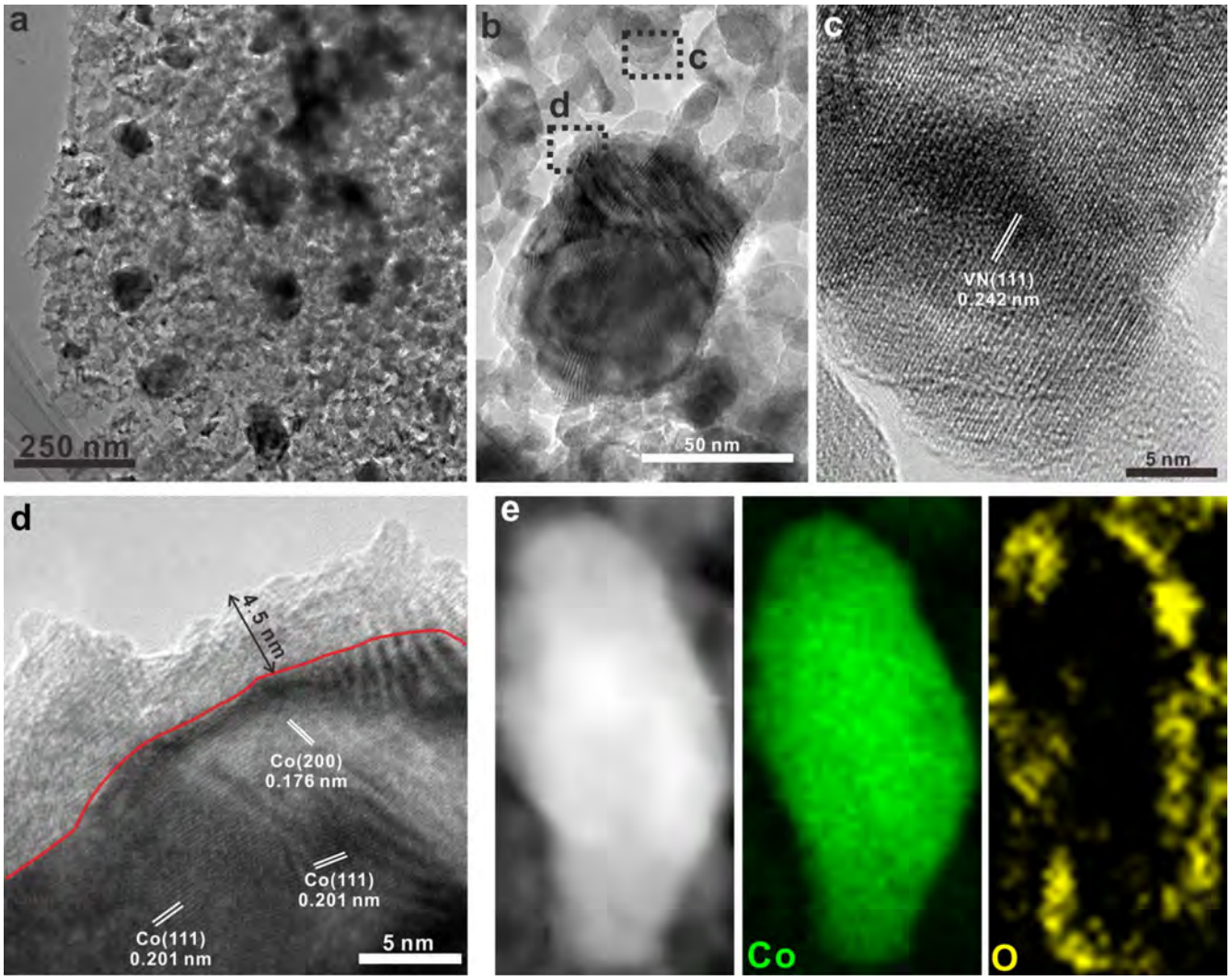

Fig. 3. (a, b) TEM and (c, d) HR-TEM images of the Co/VN. (e) Elemental maps of Co and O of the nanoparticles embedded in the Co/VN nanosheets.

(340 mV) and other reported Co-based electrocatalysts such as ε-Co NPs (473 mV) [29], Co_3O_4 (534 mV) [40], Co_3O_4/SWNTs (590 mV) [41], $NiCo_2S_4$@N/SrGO (470 mV) [42], $NiCo_2O_4$/G (440 mV) [43], and even competitive to those of Co_3O_4-RGO (310 mV) [10] and CoO-N-CG (340 mV) [44] which are considered to deliver the best performance among carbon-supported Co-based OER electrocatalysts so far as shown in Table 1. Even when the current density is up to 200 mA cm^{-2}, only a small overpotential of 412 mV is required by the Co/VN electrocatalyst. With regard to the pristine $Co_2V_2O_7$ electrocatalyst, the current density cannot reach 150 mA cm^{-2} in spite of a large overpotential of over 500 mV applied indicating the significant improvement in the OER activity offered by the Co/VN electrocatalyst after ammonia nitridation of $Co_2V_2O_7$ arising from *in situ* segregation of highly dispersed Co nanoparticles on conductive VN nanosheets with more exposed active sites. It is confirmed by the electrochemical active surface area (ECSA) measurement (Fig. S8) showing that the ECSA of Co/VN is about 10% larger than that of $Co_2V_2O_7$. To further understand the advantage of this novel structure, a control experiment was conducted by taking the mixture of metallic Co and porous VN nanosheets (Co+VN) as a comparative study, which was prepared by mixing the two components with a molar ratio of 1:1 in a typical way as carbon supported catalysts. The polarization curves and Tafel plots of the Co/VN nanosheets, Co+VN mixture, and pure VN nanosheets [30] in Fig. S9 show that pure VN is inferior to both Co/VN and Co+VN. In addition, Co/VN is better as reflected by the overpotential and Tafel slope compared to Co+VN, suggesting the way of combining Co and VN has a large impact on the OER performance. The *in situ* segregated Co nanoparticles embedded in VN nanosheets deliver better OER performance than the simple and typical mixture with the same composition on account of the small contact resistance and fast electron transfer between metallic Co and VN nanosheets in Co/VN. There are two anodic peaks in the polarization curve of Co/VN electrocatalyst at ~1.15 and ~1.4 V *vs*. RHE as shown in Fig. S10 resulting from oxidation of Co(II) to Co(III) and Co(III) to Co(IV), respectively, being consistent with previous literature [19,29,45]. During the electrochemical measurement in KOH, the metallic Co nanoparticles are further oxidized into Co(IV). They have similar OER activity as metallic Co [29] and consequently, the core metallic Co with high electronic conductivity enhances the OER activity further.

To further elucidate the effects of ammonia nitridation conditions on the OER performance, different annealing temperature and time are investigated and the results are displayed in Fig. S11. The overpotentials vary with the annealing temperature and time. When the annealing temperature is less than 550 °C and time is below 3 h, vanadate cannot be converted into Co/VN completely (Fig. S4) resulting in relatively larger overpotentials. When the annealing temperature is higher than 550 °C and time is more than 3 h, all the vanadate is converted into Co/VN (Fig. S4) producing a stable catalyst. Therefore, in order to achieve the optimal OER performance, a temperature of 550 °C and time duration of 3 h are adopted in ammonia nitridation.

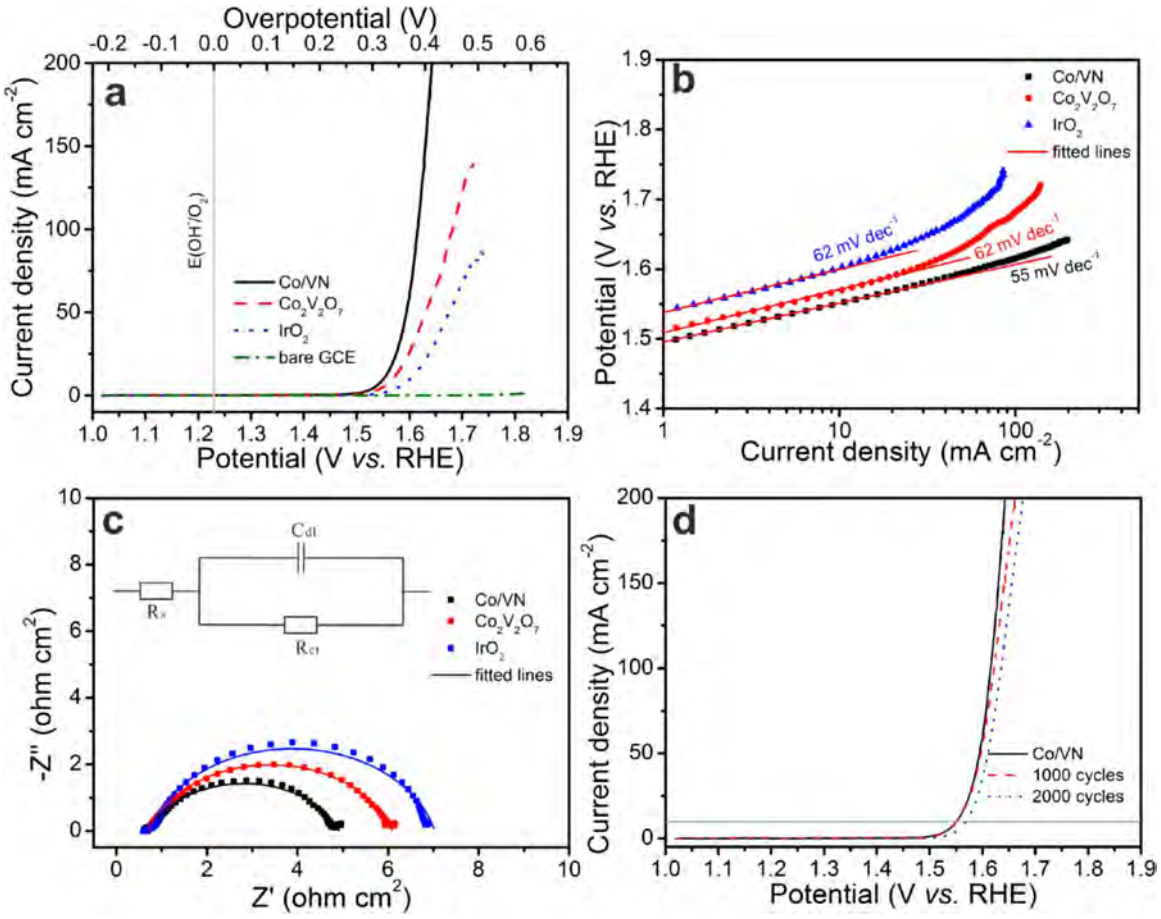

Fig. 4. (a) Polarization curves of Co/VN, $Co_2V_2O_7$, and commercial IrO_2 electrocatalysts compared to bare GCE. (b) Corresponding Tafel plots of Co/VN, $Co_2V_2O_7$, and commercial IrO_2 electrocatalysts. (c) Nyquist plots of Co/VN, $Co_2V_2O_7$, and commercial IrO_2 electrocatalysts with inset showing the electrical equivalent circuit used to simulate the Nyquist plots, where R_s is the electrolyte resistance, R_{ct} is the charge-transfer resistance, and C_{dl} represents the double-layer capacitance. (d) Stability evaluation of the Co/VN showing the polarization curves before and after CV cycling.

The Tafel plots of the Co/VN, $Co_2V_2O_7$, and commercial IrO_2 electrocatalysts are analyzed to study the OER kinetics. The Tafel slopes are determined from the Tafel equation $\eta = b \times \log j + a$, where j is the current density and b is the Tafel slope as shown in Fig. 4b. The corresponding Tafel slope of the Co/VN electrocatalyst is only 55 mV dec^{-1} (Table 1) and smaller than that of 62 mV dec^{-1} of both hydrothermal $Co_2V_2O_7$ and commercial IrO_2. It is also much smaller than those of some reported Co-based electrocatalysts and even smaller than those of Co_3O_4-RGO (67 mV dec^{-1}) [10] and CoO-N-CG (71 mV dec^{-1}) [44] which are generally considered to have the best OER properties among carbon-supported Co-based electrocatalysts (Table 1). The linear range of the Co/VN electrocatalyst in the Tafel plot extends to a large current density of ~100 mA cm^{-2} from a small current density of 1 mA cm^{-2}, revealing ultrafast charge transfer through the catalyst, which is attributed to the good contact between the metallic Co and conductive VN substrate, small contact resistance,

Table 1
Overpotentials and Tafel slopes of Co/VN, $Co_2V_2O_7$, and commercial IrO_2 electrocatalysts with *iR* correction in this work and comparison with representative Co-based OER electrocatalysts.

Catalyst	Refs.	Mass loading [mg cm^{-2}]	Electrolyte	Overpotential [mV]			Tafel slope [mV dec^{-1}]
				η_{10}[a]	η_{100}	η_{200}	
Co/VN	This work	0.28	1 M KOH	320	385	412	55
$Co_2V_2O_7$	This work	0.28	1 M KOH	340	452	–	62
IrO_2	This work	0.28	1 M KOH	370			62
Co_3O_4/N-rmGO	[10]	0.24	1 M KOH	310	–	–	67
N-CG-CoO	[44]	0.7	1 M KOH	340	–	–	71
ε-Co NPs	[29]	1	1 M KOH	473	584	655	–
Co_3O_4	[40]	1	1 M KOH	534	636		47 ± 7
Co_3O_4/SWNTs	[41]	0.05	1 M KOH	~590	–	–	104
Co-NPs	[45]	0.2	0.1 M KOH	390	–	–	–
Co/N-C-800	[46]	0.25	0.1 M KOH	371	–	–	61.4
$NiCo_2S_4$@N/SrGO	[42]	0.283	0.1 M KOH	470	–	–	–
$NiCo_2O_4$/G	[43]	0.4	0.1 M KOH	~440	–	–	164
NG-NiCo	[47]	–	0.1 M KOH	–	–	–	614

[a] Overpotential at current density of 10 mA cm^{-2}.

as well as rapid charge transfer between the Co core and VN nanosheets. The electrochemical impedance spectra (EIS) provide further evidence to the fast charge transfer as shown in Fig. 4c. The Nyquist plot (fitted with the electrical equivalent circuit in the inset of Fig. 4c) shows that the charge transfer resistance of the Co/VN electrocatalyst is 4.2 Ω cm^2 that is smaller than those of $Co_2V_2O_7$ and commercial IrO_2 catalysts (Table S1).

The stability is crucial to water splitting. Fig. 4d shows the stability of the Co/VN electrocatalysts by recording the polarization curves before and after certain CV cycles. The overpotential shows no obvious shift at a current density of 100 mA cm^{-2} and a mere 20 mV shift of 200 mA cm^{-2} is observed after 1000 CV cycles. After cycling for 2000 cycles, the overpotential shifts by only 34 mV at a current density of 200 mA cm^{-2}. The excellent stability results from the good adhesion and contact between the metallic Co and conductive VN substrate thereby preventing loss and aggregation of the embedded Co nanoparticles on the VN nanosheet substrate.

4. Conclusion

Highly active metallic Co nanoparticles are embedded in conductive VN nanosheets by ammonia nitridation of hydrothermally prepared $Co_2V_2O_7$ nanosheets. Owing to *in situ* segregation of Co from cobalt vanadate, the Co nanoparticles are distributed uniformly and bond tightly to the VN substrate. The Co/VN electrocatalyst shows an overpotential of 320 mV at a current density of 10 mA cm^{-2} and a small Tafel slope of 55 mV dec^{-1}. The electrocatalyst also has excellent stability in OER showing a shift of only 34 mV after 2000 CV cycles at a current density of 200 mA cm^{-2}. The strong adhesion between the Co nanoparticles and VN substrate prevents the particles from falling off and aggregating. The precious-metal-free Co/VN nanosheets with outstanding OER performance and a low cost are promising electrocatalysts in high-efficiency OER in alkaline media.

Acknowledgements

This work was financially supported by the National Natural Science Foundation of China (Nos. 51504171 and 51572100), Natural Science Foundation of Hubei Province (No. 2015CFA116), and the City University of Hong Kong Applied Research Grant (ARG) No. 9667122.

Appendix A. Supplementary material

Supplementary data associated with this article can be found in the online version at doi:10.1016/j.nanoen.2017.02.016.

References

[1] R. Subbaraman, D. Tripkovic, D. Strmcnik, K.-C. Chang, M. Uchimura, A.P. Paulikas, V. Stamenkovic, N.M. Markovic, Science 334 (2011) 1256–1260.
[2] N. Armaroli, V. Balzani, Angew. Chem. Int. Ed. 46 (2007) 52–66.
[3] J.A. Turner, Science 305 (2004) 972–974.
[4] H.G. Sanchez Casalongue, M.L. Ng, S. Kaya, D. Friebel, H. Ogasawara, A. Nilsson, Angew. Chem. Int. Ed. 53 (2014) 7169–7172.
[5] Y.-H. Fang, Z.-P. Liu, J. Am. Chem. Soc. 132 (2010) 18214–18222.
[6] H.N. Nong, H.S. Oh, T. Reier, E. Willinger, M.G. Willinger, V. Petkov, D. Teschner, P. Strasser, Angew. Chem. Int. Ed. 54 (2015) 2975–2979.
[7] M.G. Walter, E.L. Warren, J.R. McKone, S.W. Boettcher, Q. Mi, E.A. Santori, N.S. Lewis, Chem. Rev. 110 (2010) 6446–6473.
[8] J. Wang, H. Zhong, Y. Qin, X. Zhang, Angew. Chem. Int. Ed. 52 (2013) 5248–5253.
[9] L.G. Feng, K. Li, J.F. Chang, C.P. Liu, W. Xing, Nano Energy 15 (2015) 462–469.
[10] Y. Liang, Y. Li, H. Wang, J. Zhou, J. Wang, T. Regier, H. Dai, Nat. Mater. 10 (2011) 780–786.
[11] M.W. Kanan, D.G. Nocera, Science 321 (2008) 1072–1075.
[12] V. Artero, M. Chavarot-Kerlidou, M. Fontecave, Angew. Chem. Int. Ed. 50 (2011) 7238–7266.
[13] J. Masa, W. Xia, I. Sinev, A. Zhao, Z. Sun, S. Grützke, P. Weide, M. Muhler, W. Schuhmann, Angew. Chem. Int. Ed. 53 (2014) 8508–8512.
[14] M. Zhang, M. de Respinis, H. Frei, Nat. Chem. 6 (2014) 362–367.
[15] F. Jiao, H. Frei, Angew. Chem. Int. Ed. 48 (2009) 1841–1844.
[16] X.L. Yang, H.N. Li, A.Y. Lu, S.X. Min, Z. Idriss, M.N. Hedhili, K.W. Huang, H. Idriss, L.J. Li, Nano Energy 25 (2016) 42–50.
[17] A. Zhao, J. Masa, W. Xia, A. Maljusch, M.-G. Willinger, G. Clavel, K. Xie, R. Schlögl, W. Schuhmann, M. Muhler, J. Am. Chem. Soc. 136 (2014) 7551–7554.
[18] Y. Hou, J.Y. Li, Z.H. Wen, S.M. Cui, C. Yuan, J.H. Chen, Nano Energy 12 (2015) 1–8.
[19] B.S. Yeo, A.T. Bell, J. Am. Chem. Soc. 133 (2011) 5587–5593.
[20] C. Yuan, J. Li, L. Hou, X. Zhang, L. Shen, X.W.D. Lou, Adv. Funct. Mater. 22 (2012) 4592–4597.
[21] J. Yin, L. Wang, C.G. Tian, T.X. Tan, G. Mu, L. Zhao, H.G. Fu, Chem. Eur. J. 19 (2013) 13979–13986.
[22] M.H. Yang, Z.M. Cui, F.J. DiSalvo, Chem. Commun. 48 (2012) 10502–10504.
[23] C.H. Winter, V.C. Viejo, J.W. Proscia, Single-source precursors to vanadium nitride thin films, MRS Proc. (1993) 109.
[24] S. Oyama, Catal. Today 15 (1992) 179–200.
[25] Y.Q. Cong, H.S. Park, H.X. Dang, F.R.F. Fan, A.J. Bard, C.B. Mullins, Chem. Mater. 24 (2012) 579–586.
[26] R. Kojima, K. Aika, Appl. Catal. A-Gen. 215 (2001) 149–160.
[27] X. Xiao, X. Peng, H. Jin, T. Li, C. Zhang, B. Gao, B. Hu, K. Huo, J. Zhou, Adv. Mater. 25 (2013) 5091–5097.
[28] D.W. Kim, D.K. Lee, S.K. Ihm, Catal. Lett. 43 (1997) 91–95.
[29] N.H. Chou, P.N. Ross, A.T. Bell, T.D. Tilley, ChemSusChem 4 (2011) 1566–1569.
[30] X. Peng, W. Li, L. Wang, L. Hu, W. Jin, A. Gao, X. Zhang, K. Huo, P.K. Chu, Electrochim. Acta 214 (2016) 201–207.
[31] I.K. Milad, K.J. Smith, P.C. Wong, K.A.R. Mitchell, Catal. Lett. 52 (1998) 113–119.
[32] D. Choi, G.E. Blomgren, P.N. Kumta, Adv. Mater. 18 (2006) 1178–1182.
[33] B. Gao, X. Li, X. Guo, X. Zhang, X. Peng, L. Wang, J. Fu, P.K. Chu, K. Huo, Adv. Mater. Interfaces 2 (2015) 1500211.
[34] X.H. Zhou, C.Q. Shang, L. Gu, S.M. Dong, X. Chen, P.X. Han, L.F. Li, J.H. Yao, Z.H. Liu, H.X. Xu, Y.W. Zhu, G.L. Cui, ACS Appl. Mater. Interfaces 3 (2011) 3058–3063.
[35] X. Peng, L. Hu, L. Wang, X. Zhang, J. Fu, K. Huo, S.L.Y. Lee, K.-Y. Wong, P.K. Chu, Nano Energy 26 (2016) 603–609.
[36] S. Todorova, H. Kolev, J.P. Holgado, G. Kadinov, C. Bonev, R. Pereniguez, A. Caballero, Appl. Catal. B-Environ. 94 (2010) 46–54.
[37] L. Fu, Z.M. Liu, Y.Q. Liu, B.X. Han, P.G. Hu, L.C. Cao, D.B. Zhu, Adv. Mater. 17 (2005) 217–221.
[38] M. Dominguez, E. Taboada, H. Idriss, E. Molins, J. Llorca, J. Mater. Chem. 20 (2010) 4875–4883.
[39] C.C. McCrory, S. Jung, J.C. Peters, T.F. Jaramillo, J. Am. Chem. Soc. 135 (2013) 16977–16987.
[40] A.J. Esswein, M.J. McMurdo, P.N. Ross, A.T. Bell, T.D. Tilley, J. Phys. Chem. C 113 (2009) 15068–15072.
[41] J. Wu, Y. Xue, X. Yan, W.S. Yan, Q.M. Cheng, Y. Xie, Nano Res. 5 (2012) 521–530.
[42] Q. Liu, J.T. Jin, J.Y. Zhang, ACS Appl. Mater. Interfaces 5 (2013) 5002–5008.
[43] D.U. Lee, B.J. Kim, Z.W. Chen, J. Mater. Chem. A 1 (2013) 4754–4762.
[44] S. Mao, Z. Wen, T. Huang, Y. Hou, J. Chen, Energy Environ. Sci. 7 (2014) 609–616.
[45] L.H. Wu, Q. Li, C.H. Wu, H.Y. Zhu, A. Mendoza-Garcia, B. Shen, J.H. Guo, S.H. Sun, J. Am. Chem. Soc. 137 (2015) 7071–7074.
[46] Y.H. Su, Y.H. Zhu, H.L. Jiang, J.H. Shen, X.L. Yang, W.J. Zou, J.D. Chen, C.Z. Li, Nanoscale 6 (2014) 15080–15089.
[47] S. Chen, J.J. Duan, M. Jaroniec, S.Z. Qiao, Angew. Chem. Int. Ed. 52 (2013) 13567–13570.

Xiang Peng received his Master's degree in materials science from Wuhan University of Science and Technology in 2014. He is presently a Ph.D. candidate under the supervision of Prof. Paul K. Chu in Department of Physics and Materials Science, City University of Hong Kong. His research focuses on synthesis of functional nanomaterials and fabrication of electrochemical energy devices for supercapacitors, Li-ion batteries, and electrocatalysis applications.

Lei Wang earned his B.S. degree in physics from Huazhong University of Science and Technology (HUST) in 2012. He is currently pursuing his Ph.D. in the Wuhan National Laboratory for Optoelectronics (WNLO) at Huazhong University of Science and Technology (HUST) under the supervision of Prof. Kaifu Huo. His research is on the synthesis of synthesis and characterization of nanostructured electrode architectures and materials for electrochemical energy conversion and storage.

Liangsheng HU received his B.S. and M.S. from Wuhan University of Science and Technology in 2007 and 2011, respectively. Currently, he is a Ph.D. candidate in chemistry of The Hong Kong Polytechnic University. His research interests focus on the synthesis and application of functional nanomaterials for (electro)photochemical energy conversion and storage.

Yong Li received his B.S. and M.S. from Wuhan University of Science and Technology in 2011 and 2014, respectively. He worked at Shenzhen Institutes of Advanced Technology, Chinese Academy of Sciences from 2014 to 2016. Currently, he works at The Hong Kong Polytechnic University as Research Assistant. His research interests focus on nanostructured materials for electrocatalysis and electrochemical sensors.

Biao Gao received his M.S. and Ph.D. in materials science from Wuhan University of Science and Technology in 2012 and 2016, respectively. He is a lecturer in the State Key Laboratory of Refractories and Metallurgy at Wuhan University of Science and Technology. His main research activity involves nanostructures for electrochemical energy storage.

Hao Song received his B.S. in materials science from Wuhan University of Science and Technology in 2015 and is a M.S. candidate under the supervision of Prof. Jijiang Fu in the State Key Laboratory of Refractories and Metallurgy at Wuhan University of Science and Technology. His main research activity involves nanostructures for supercapacitors.

Chao Huang received his B.S. in materials science from Wuhan University of Science and Technology in 2014 and presently is a M.S. candidate in the State Key Laboratory of Refractories and Metallurgy at Wuhan University of Science and Technology. His research mainly focuses on nanomaterials for energy storage and conversion.

Xuming Zhang received his Ph.D. in materials science and engineering from City University of Hong Kong in 2015 and worked for one year as a senior research associate in the Plasma Laboratory at City University of Hong Kong. He is now a professor in Wuhan University of Science and Technology. His research interests are synthesis of nanomaterials for electrochemical sensors and electrochemical energy storage devices.

Jijiang Fu received his B.S. in chemistry from Nanchang University in 1993 and Ph.D. in physical chemistry from Nanjing University (China) in 2005. He is currently professor of materials science at Wuhan University of Science and Technology. His current research focuses on bioactive nanomaterials and nanostructured electrode materials for electrochemical biosensors and energy storage devices.

Kaifu Huo received his B.S. in applied chemistry from China University of Petroleum in 1997 and Ph.D. in physical chemistry from Nanjing University (China) in 2004. Currently, he is a professor in the National Laboratory for Optoelectronics at Huazhong University of Science and Technology. He is an associate editor of Nanoscience and Nanotechnology Letters (NNL). He has authored/co-authored more than 100 papers in international refereed journals which have been cited more than 3000 times (current H-index=30). His main research activities encompass bioactive nanomaterials and nanostructured electrode materials for electrochemical biosensors and energy storage devices.

Paul K. Chu received his Ph.D. in Chemistry from Cornell University. He is Chair Professor of Materials Engineering in the Department of Physics and Materials Science at City University of Hong Kong. He is Fellow of the American Physical Society (APS), American Vacuum Society (AVS), Institute of Electrical and Electronics Engineers (IEEE), Materials Research Society (MRS), and Hong Kong Institution of Engineers (HKIE). He is also Fellow and member of the processing engineering committee of the Hong Kong Academy of Engineering Sciences (HKAES). His research interests are quite diverse encompassing plasma surface engineering, materials science and engineering, surface science, and functional materials. He is a highly cited researcher in materials science according to Thomson Reuters.

Supporting Information

In situ segregation of cobalt nanoparticles on VN nanosheets *via* nitriding of $Co_2V_2O_7$ nanosheets as efficient oxygen evolution reaction electrocatalysts

Xiang Peng[a], Lei Wang[b], Liangsheng Hu[c], Yong Li[c], Biao Gao[d], Hao Song[d], Chao Huang[a,d], Xuming Zhang[d], Jijiang Fu[d], Kaifu Huo*[,b], Paul K. Chu*[,a]

[a] Department of Physics and Materials Science, City University of Hong Kong, Tat Chee Avenue, Kowloon, Hong Kong, China.

E-mail: paul.chu@cityu.edu.hk, fax: +852 34420538, Tel.: +852 34427724

[b] Wuhan National Laboratory for Optoelectronics, Huazhong University of Science and Technology, Wuhan 430074, China.

E-mail: kfhuo@hust.edu.cn

[c] Department of Applied Biology and Chemical Technology and the State Key Laboratory of Chirosciences, The Hong Kong Polytechnic University, Hung Hom, Kowloon, Hong Kong, China

[d] The State Key Laboratory of Refractories and Metallurgy, Wuhan University of Science and Technology, Wuhan 430081, China

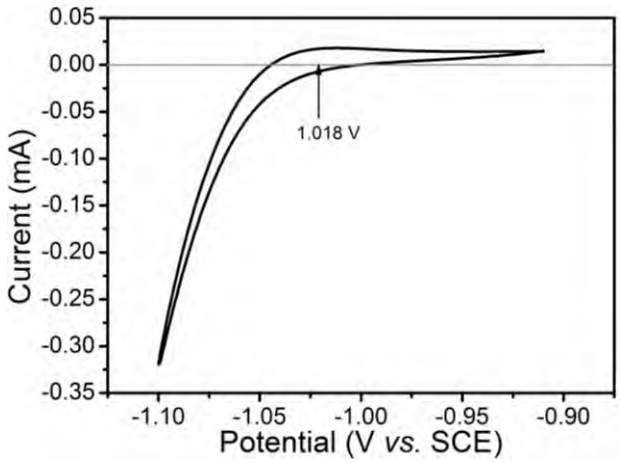

Figure S1 Calibration of the reference to RHE in 1 M KOH. The calibration was presented in the high purity hydrogen saturated electrolyte with a Pt wire as working electrode. The cyclic voltammetry was recorded at scan rate of 1 mV s^{-1}, and the average of the two potentials at which the current crossed zero was taken to be the thermodynamic potential for the hydrogen electrode reaction.

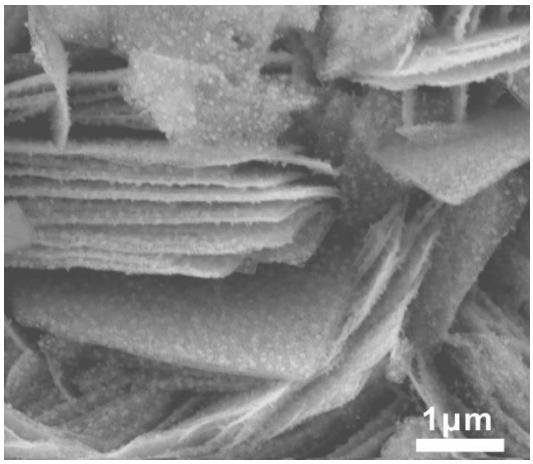

Figure S2 FE-SEM image of Co/VN.

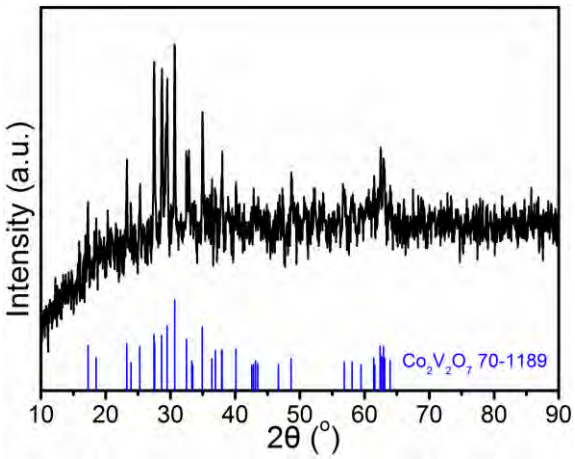

Figure S3 XRD patterns of the hydrothermal product after annealing in air at 550 °C compared to the standard X-Ray diffraction pattern of $Co_2V_2O_7$ (JCPDS 70-1189).

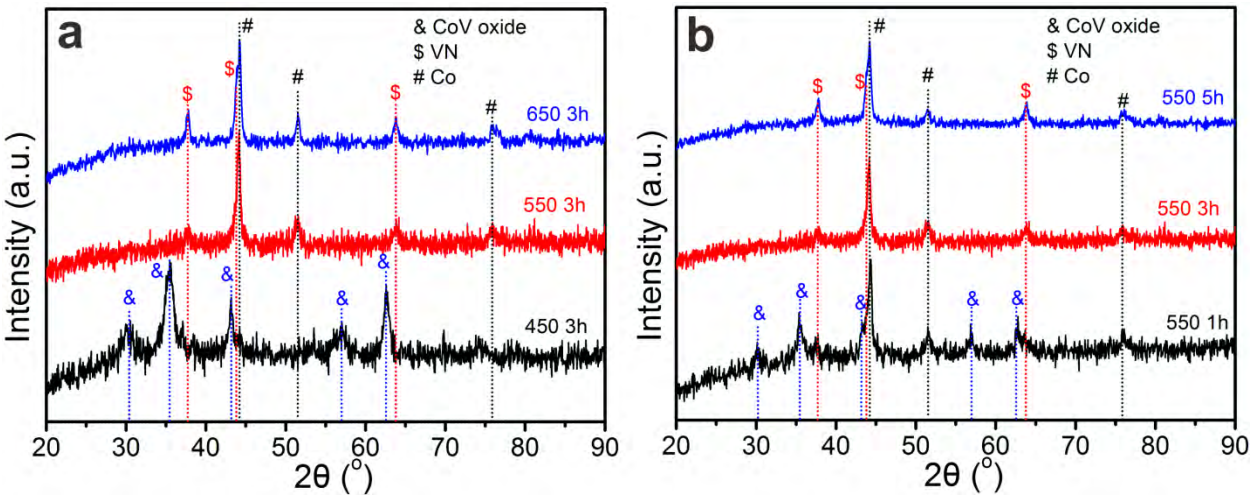

Figure S4 XRD patterns of the products annealed (a) at different temperature and (b) for different time duration.

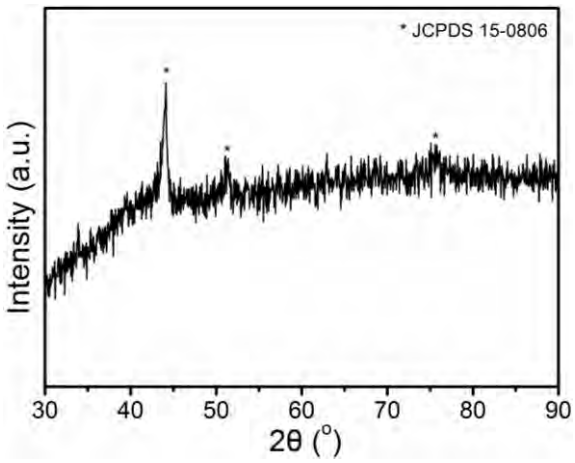

Figure S5 XRD patterns of the product prepared hydrothermally followed by ammonia nitridation without V_2O_5 as the precursor.

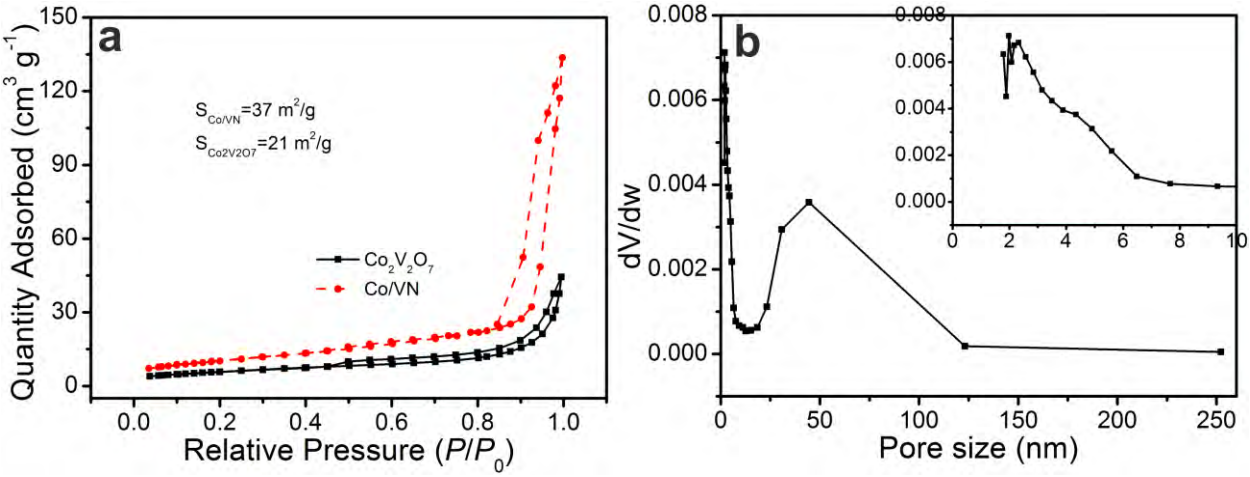

Figure S6 (a) N_2 adsorption/desorption isotherms of Co/VN and $Co_2V_2O_7$. (b) Corresponding pore size distribution of Co/VN with the inset showing the pore size in the range between 0 and 10 nm.

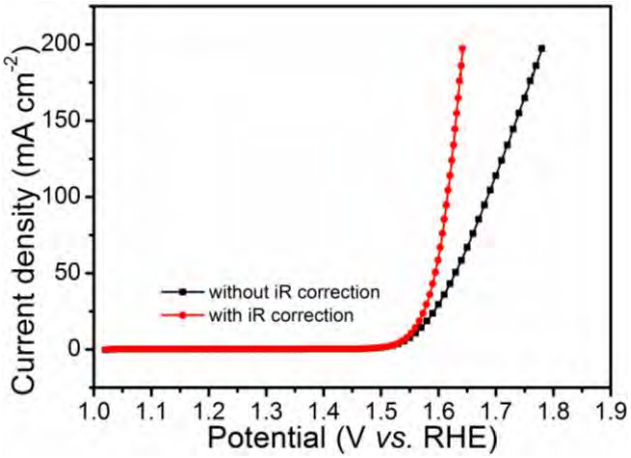

Figure S7 Polarization curves of the Co/VN electrocatalyst with and without *iR* correction.

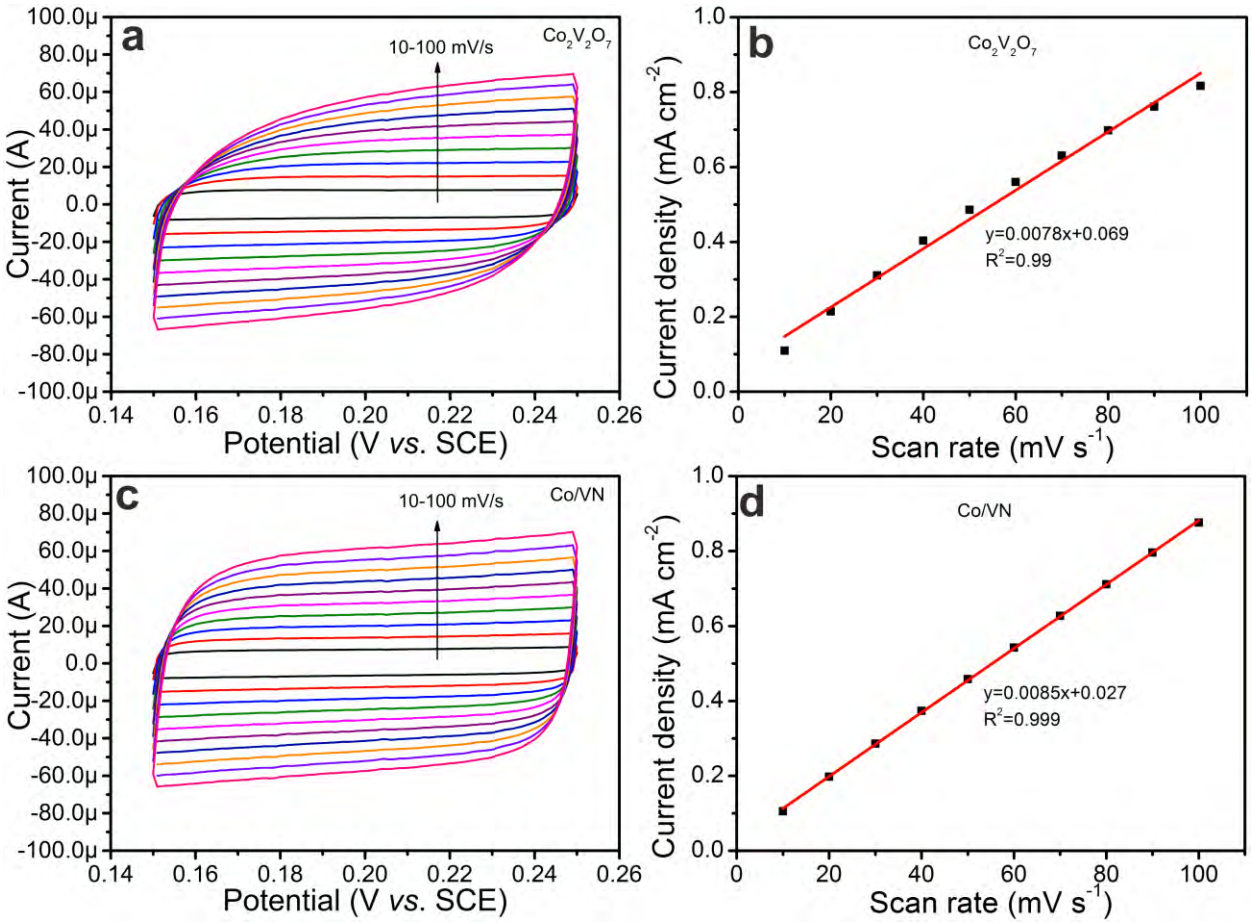

Figure S8 (a) and (c) Electrochemically active surface areas (ECSA) determined by the double layer capacitance (C_{DL}) measurements from cyclic voltammetry (CV) in 1 M KOH from the $Co_2V_2O_7$ and Co/VN catalysts at scanning rates between 10 and 100 mV s^{-1}. (b) and (d) Anodic current densities at 0.2 V *vs.* SCE to correlate the scanning rates with current densities. The ECSA is proportional to C_{DL} which is obtained by the relationship $I = C_{DL}v$.[1]

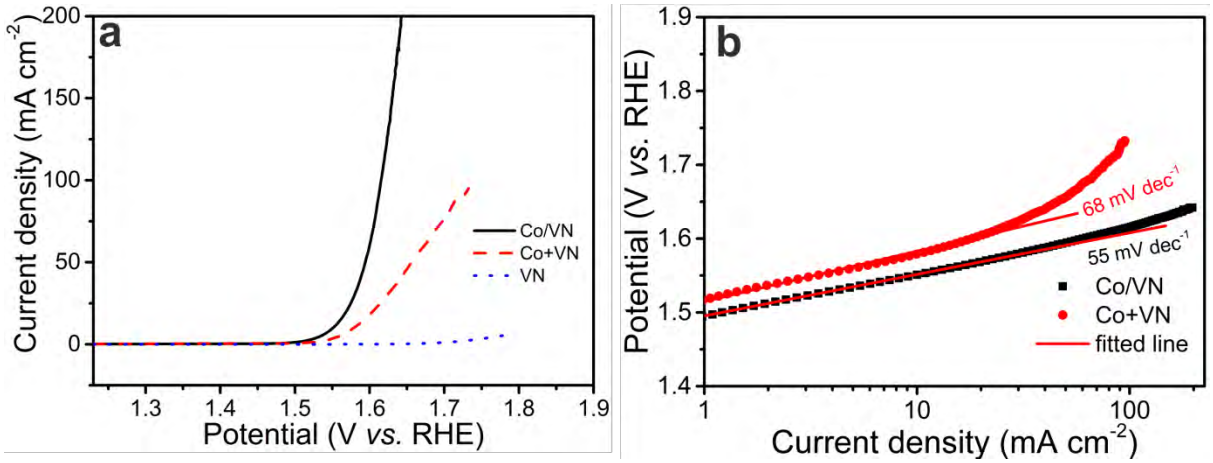

Figure S9 (a) Polarization curves and (b) Tafel plots of Co/VN, Co+VN and VN. The VN nanosheets are prepared according to our previous report [2].

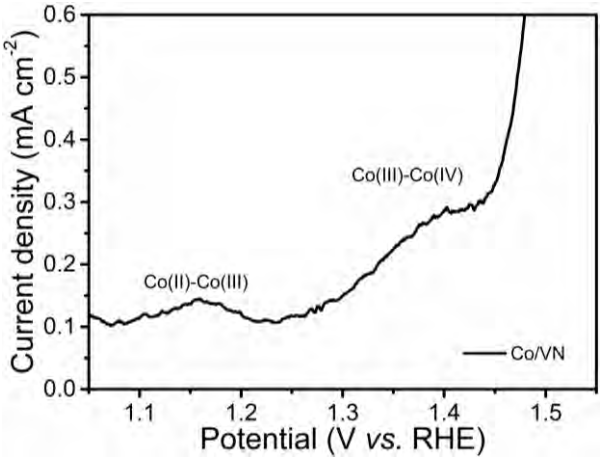

Figure S10 Magnified polarization curve of Co/VN to illustrate oxidation of Co preceding OER.

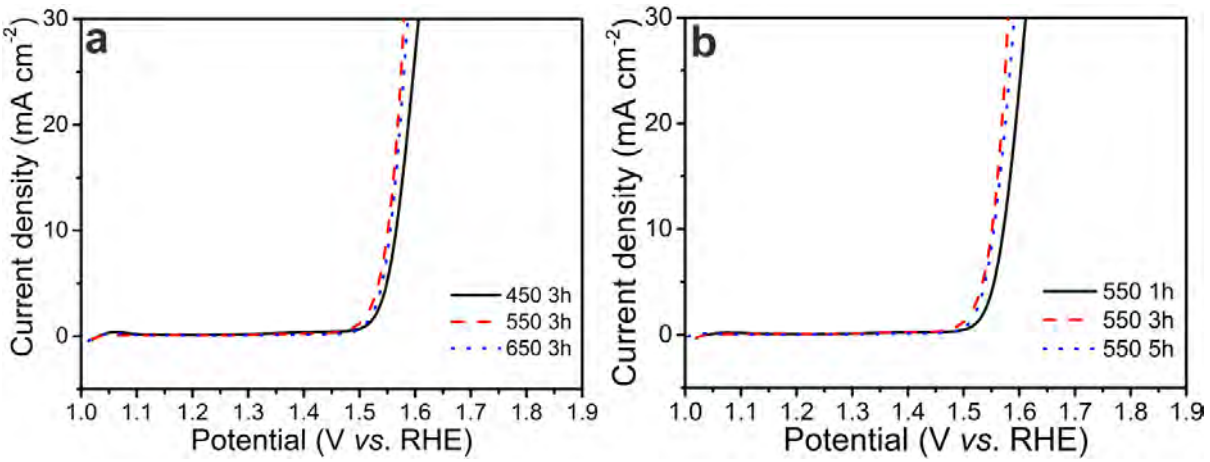

Figure S11 Polarization curves of the products annealed (a) at different temperature and (b) for different time duration.

Table S1 Fitted parameters of the Co/VN, $Co_2V_2O_7$, and IrO_2 electrocatalysts at a potential of 0.6 V *vs.* SCE.

Sample	R_s [ohm cm^2]	R_{ct} [ohm cm^2]	*CPE* [S s^n cm^{-2}]
Co/VN	0.70	4.22	0.001831
$Co_2V_2O_7$	0.71	5.38	0.0009849
IrO_2	0.74	6.29	0.002565

References

[1] M. Ledendecker, H. Schlott, M. Antonietti, B. Meyer, M. Shalom, Adv. Energy Mater. (2016) DOI: 10.1002/aenm.201601735.

[2] X. Peng, W. Li, L. Wang, L. Hu, W. Jin, A. Gao, X. Zhang, K. Huo, P.K. Chu, Electrochim. Acta 214 (2016) 201-207.